JOURNAL OF MATERIALS SCIENCE **36** (2001) 2511–2522

Reactivity of layered vanadium pentoxide hydrate with ultrafine metal oxide, TiO_2 and ZrO_2, particles in an aqueous system

S. KITTAKA*, K. MATSUNO, K. TANAKA
Department of Chemistry, Faculty of Science, Okayama University of Science, 1-1 Ridaicho, Okayama 700-0005, Japan
E-mail: kittaka@chem.ous.ac.jp

Y. KURODA
Department of Chemistry, Faculty of Science, Okayama University, Tsushima, Okayama 700-8530, Japan

M. FUKUHARA
Department of Applied Chemistry, Faculty of Engineering, Okayama University of Science, 1-1 Ridaicho, Okayama 700-0005, Japan

The interactions between vanadium pentoxide hydrate ($V_2O_5 \cdot nH_2O$) sol and colloid solutions of ultra fine titanium dioxide TiO_2 and zirconium dioxide particles ZrO_2 were studied. When mixed with an intrinsic $V_2O_5 \cdot nH_2O$ sol, TiO_2 particles in the mixed sol are sandwiched by $V_2O_5 \cdot nH_2O$ layer sheets to form intercalation compounds. An Interlayer distance of $V_2O_5 \cdot nH_2O$ was increased by this treatment and the surface area was also increased from 7.9 $m^2\ g^{-1}$ for the $V_2O_5 \cdot nH_2O$ to ca. 50 $m^2\ g^{-1}$. When the TiO_2 sol was contacted with K-type $V_2O_5 \cdot nH_2O$, microporous nature appeared in the sample and the surface area incrased up to ca. 100 $m^2\ g^{-1}$. The porous structure was maintained up to 300°C, above which materials were separated into two phases, anhydrous V_2O_5 and anatase type TiO_2. Ultrafine ZrO_2 particles were intercalated stoichiometrically in both intrinsic and K-type $V_2O_5 \cdot nH_2O$ giving ZrO_2-$V_2O_5 \cdot nH_2O$ for all the mixing ratios from $ZrO_2/V_2O_5 = 5$ to 20. Physico-chemical properties were almost unvaried and the materials were nonporous. Their surface areas are around 50 $m^2\ g^{-1}$ for the former and around 60 $m^2\ g^{-1}$ for the latter. The layered structure was maintained up to 300°C above which the sample was crystallized into ZrV_2O_7. The reaction temperature is about 150°C lower than that the heated mixture of ZrO_2 and V_2O_5 powders. The electron microscope observations of the prepared materials showed that the number of the stacked layers was decreased from more than 10 sheets for the sample before intercalation to about 2–4 sheets by exfoliation. This indicates that $V_2O_5 \cdot nH_2O$ is exfoliated by ion exchangeably reacting to ultrafine titanium oxide and zirconium oxide particles.

1. Introduction

Vanadium pentoxide hydrate ($V_2O_5 \cdot nH_2O$) is a colloidal particle with an orthorhombic layered structure like smectite-type clays and swells in the presence of water [1, 2]. The particles carry negative surface charges in water, and have cation-exchangeability and adsorbability for the polar molecules [3–5]. Thus, this makes us hopeful that we can form an intercalation compound having various physico-chemical properties.

One possibility for this sample is a pillar formation to produce porous material. In the case of smectite type clays, ultrafine metal oxide particles can be intercalated to form pillars leading to porous material. The introduction of positively charged TiO_2 particles or clusters in the layered structure of clay minerals has been developed successfully by some groups to form porous materials [6–8]. There were several successes in the introduction of ZrO_2 particles prepared by the hydrolysis of $ZrOCl_2$ into clays which has been understood that $[Zr_4(OH)_{12}]^{2+}$ clusters were introduced [9, 10]. However, intercalation of fine particles in the $V_2O_5 \cdot nH_2O$ has not been studied on this line.

An anhydrous V_2O_5 is historically well known for its various practical uses as catalysts for re-dox reactions as impregnated form on the various metal oxide substrates like SiO_2, TiO_2, and ZrO_2 etc, in which

* Author to whom all correspondence should be addressed.

catalytic activity is strongly affected by the nature of the substrates [11–15], and such activity can be expected from the variety of ionic charges of vanadium ions in the oxides. $V_2O_5 \cdot nH_2O$ is also chemically active and, in some cases, forms intercalation compound with metal ions as transition materials leading to metal vanadates [4, 16–18].

The present work aims to study how the layered structure of $V_2O_5 \cdot nH_2O$ and physico-chemical properties are modified to bring in the above properties by reactions with ultrafine TiO_2 and ZrO_2 particles. The thermal properties of the intercalation products formed were studied in comparison with the formation method of a metal vanadate by a solid reaction.

2. Experimental procedure

2.1. Materials

2.1.1. Preparation of $V_2O_5 \cdot nH_2O$ sol, TiO_2 sol, ZrO_2 sol, and K-$V_2O_5 \cdot nH_2O$

$V_2O_5 \cdot nH_2O$ sol was formed by the conventional ion-exchange polymerization method from NH_4VO_3 solution [19]. A freeze-dried sample was prepared for the intercalation experiments but gave no significant difference in the results. It has been understood that $V_2O_5 \cdot nH_2O$ layer sheets are separated from each other by swelling. When used as a host reactant, the reaction mechanism will be that they should sandwich the metal oxide particles. In order to test the effect of the starting material on the intercalation, K-$V_2O_5 \cdot nH_2O$ was prepared for the reaction. The introduced K^+ ion content was 0.32 mol per 1 mol V_2O_5 [4]. The sample thus prepared was precipitated immediately by an ion-exchange reaction, since layer stacking was contracted along the c-direction due to the enhanced ionic interactions between the layers. All the heating of the samples were conducted in air for 1 h.

TiO_2 sol was prepared at room temperature by hydrolyzing titanium tetra-isopropoxide in a 1 mol dm^{-3} HCl solution, in 200 cm^3 of which a programmed amount of alkoxide (0.05 mol) was dripped and stirred. The solution was turbid at first with small white coagulates [15]. This heterogeneous system became transparent after vigorous stirring for about 3 h. After a few hours this solution became turbid due to the crystallization of TiO_2 particles into rutile. When the transparent sol was dialyzed quickly with distilled water, a transparent gel was formed. The latter could easily be returned to a transparent sol when it was contacted with an HCl solution. This kind of gel has been understood as forming a network by connecting fine particles. Transmission electron microscopy (TEM) showed that particles obtained by freeze-drying the transparent gel are less than 3 nm. This makes us suppose that the particles in a transparent sol are smaller than this and not uniform in size. The observed specific surface area is 256 $m^2\ g^{-1}$.

ZrO_2 sol was prepared as done for the TiO_2 sol, in which tetra-n-butoxy-zirconium was hydrolyzed in an HCl solution. In contrast to TiO_2 sol, however, once the mixture became transparent it was stable and did not give precipitate. It was confirmed that the mixture is a solution of $ZrOCl_2 \cdot 8H_2O$ which was crystallized when this solution had dried. A tetra-nuclear cluster of $[Zr_4(OH)_8(H_2O)_{16}]^{8+}$ is known as a component of the crystal [20]. We could then expect the presence of poly-nuclear species, $[Zr_3(OH)_4]^{8+}$, $[Zr_4(OH)_8]^{8+}$ etc. in the acidic solution. Although the PZC of ZrO_2 particle was around 7 [21], neither sediment nor gel was formed even after dialyzing this solution close to pH 7. This means that ZrO_2 particles are quite stable with a homogeneous particle size and a positive surface charge in an acidic system. Freeze-dried sol gave amorphous particles, which cannot be identified as discrete fine particles by high resolution TEM (not shown), indicating that strong aggregation has occurred between the particles. The determined surface area was 24.7 $m^2\ g^{-1}$.

2.1.2. Intercalation of TiO_2 and ZrO_2 particles in the $V_2O_5 \cdot nH_2O$ layers

Intercalation of TiO_2 particles in the $V_2O_5 \cdot nH_2O$ was conducted by applying Yamanaka's method [7]. Varying volumes of transparent sol were dripped in the $V_2O_5 \cdot nH_2O$ sol (0.19 mol (V_2O_5)dm^{-3}) at room temperature and stirred. For more thorough mixing of the sols, mixtures were sonicated. The tested mixing ratio was from $TiO_2/V_2O_5 = 0.5$ to 20 in formal concentration ratio; the samples were named as TV-0.5–TV-20, respectively). The sediments formed were aged overnight. The sediments obtained were repeatedly washed by decantation with distilled water and sonication to remove excess TiO_2 particles from the sample surface. Then, purified sediments were freeze-dried to avoid coagulation for the following experiments.

ZrO_2 sol was reacted with the $V_2O_5 \cdot nH_2O$ sol by changing the mixing ratios, ZV = 0.1–20, and treated similarly to the system including TiO_2 particles.

2.2. Analysis of atomic compositions

Atomic compositions of the reaction products were determined by the use of ICP (Shimadzu ICPS500). Sample solutions were prepared by dissolving 35 mg of a solid sample in 2 cm^3 of 2.5 mol dm^{-3} H_2SO_4 and diluting it with distilled water to the final volume of 100 cm^3. Standard solutions for metal ions were purchased from Ishizu Seiyaku Ltd.

2.3. Crystal structures and textures

The crystal structure of the samples was studied by XRD measurements by using Rigaku RAD-2R equipped with Cu-targeted XRD tube ($\lambda = 0.15418$ nm). Wet samples were spread over the glass plate and dried spontaneously in air to orient the layered plane parallel to the glass surface. However, there appeared some weak diffraction peaks other than that for 00ℓ, which is due to the fact that the samples have been fragmented significantly. The measurements were performed in air (humidity was ca 50–60%). A transmission electron microscope (Hitachi H8100) was used to investigate the texture and the crystal structure of particles in which an accelerating voltage of electron beam was 200 kV.

2.4. Pore analyses

The microporosity of the samples was studied by N_2 adsorption at the temperature of liquid N_2. The surface

area and porosity was analyzed by BET equation and by *t*-plot analysis, respectively. In the latter, *t*-values were derived from the table for each BET c-value [22].

2.5. FT-IR measurements

The change in the interatomic vibration in the layer sheets upon intercalation of metal oxide particles was studied by FT-IR measurements in a vacuum by 100 scannings at the resolution of 4 cm^{-1} (JEOL JIR-100).

2.6. ESR measurements

The $V_2O_5 \cdot nH_2O$ is composed of 1–2% V^{4+} ions which can be a probe for the electronic structure analysis of the material by using ESR [23]. The ESR spectra of intrinsic and intercalated samples were measured after evacuation at room temperature. The apparatus used is a JEOL-FE3XG.

2.7. Thermal properties

Thermal properties of the samples were studied by use of TG-DTA (ULVAC, TGD-7000). Measurements were performed in air at the heating rate 5°C min^{-1}.

3. Results and discussion

3.1. Intercalation of ultrafine TiO_2 and ZrO_2 particles in the $V_2O_5 \cdot nH_2O$

Tables I and II show the sample names indicating the mixing ratio of metal oxide to $V_2O_5 \cdot nH_2O$ and their composition of products. With TV samples in Table I, TiO_2 composition increases slowly with mixing ratios. In the KTV samples, the TiO_2 composition is slightly larger than in the TV samples and increases with mixing ratios. In contrast, the difference between ZV and KZV samples is less marked (Table II). The ZrO_2 composition to V_2O_5 in ZV is roughly 1 : 1 in molar ratio. The smaller cluster size of the ZrO_2 particles seems to satisfy the stoichiometric requirements.

The difference of the reactivity of TiO_2 and ZrO_2 sols may be ascribed to the differences in their reactivities in the sol before mixing. The particle size of ZrO_2 is very stable and does not change with time even after removing HCl by dialysis, while the TiO_2 particles coagulated and crystallized after a few hours even in the presence of HCl. Then it is reasonable to predict that particle size distributions present different effects on the intercalation processes.

Figs 1 and 2 show XRD patterns of the samples TV, KTV, ZV, and KZV, together with the $V_2O_5 \cdot nH_2O$ and K-$V_2O_5 \cdot nH_2O$. Sharp harmonic 00ℓ peaks for the intrinsic $V_2O_5 \cdot nH_2O$ were little changed by ion-exchangeable intercalation of K^+. Layered structure was markedly affected by the interaction with TiO_2 and ZrO_2 sols to increase interlayer distance and loose crystallinity. In the KTV samples, the line broadening of a single XRD peak is slightly larger than that for the TV samples. Mean interlayer spacing is larger for the former than the latter. These facts reflect the higher accessibility of larger TiO_2 particles in KTV samples.

The structural features are visualized also by an electron microscope as shown in Fig. 3a–e. The pure $V_2O_5 \cdot nH_2O$ sample has a thick uniform layer stacking, (Fig. 3a), indicating that $V_2O_5 \cdot nH_2O$ sheets are not so much far from each other and interacting with each other through weak force even in a sol. When dilute TiO_2 sol is contacted with $V_2O_5 \cdot nH_2O$, a rather compact layered structure and ambiguous filmy solid can be seen simultaneously. With increase in TiO_2 concentration, rough films appeared (Fig. 3b) and a compact layered part was lost giving broadened layer stacking (Fig. 3c). This is parallel with the displacement of the XRD peak to lower angles and broadening with increase in TiO_2 sol concentration. The product particles formed are fragmented. The texture changes were apparently similar between TV and KTV samples.

When ZrO_2 particles were introduced, compact layer stacking was lost immediately even with dilute ZrO_2 sol and fragmented significantly: filmy sheets were found in both ZV and KZV systems as seen in Fig. 3d and e, respectively. The electron microscopic observation and line broadening analyses of the XRD pattern using the Sherrer equation makes us estimate that each sheet is composed of about 3 or 4 unit layers. That is,

TABLE I Compositions and surface areas of parameters of $V_2O_5 \cdot nH_2O$ and K-$V_2O_5 \cdot nH_2O$ intercalated with TiO_2 fine particles

TV			KTV			
Samples	TiO_2/V_2O_5	$S/m^2\ g^{-1}$	Samples	K/V_2O_5	TiO_2/V_2O_5	$S/m^2\ g^{-1}$
$V_2O_5 . nH_2O$	0	7.90	K-$V_2O_5 . nH_2O$	0.32	----	----
TV-1	0.854	40.4	KTV-1	0.180	0.778	----
TV-4	1.34	49.4	KTV-5	0.03	1.69	100
TV-10	1.56	57.3	KTV-10	0.01	1.70	86.9
TV-20	1.66	60.1	KTV-20	0.008	2.00	79.8

TABLE II Compositions and surface areas of parameters of $V_2O_5 \cdot nH_2O$ and K-$V_2O_5 \cdot nH_2O$ intercalated with ZrO_2 fine particles

ZV			KZV			
ZrO_2/V_2O_5	ZrO_2/V_2O_5	$S/m^2\ g^{-1}$	Samples	K/V_2O_5	ZrO_2/V_2O_5	$S/m^2\ g^{-1}$
ZV-1	0.698	----	KZV-1	0.0072	0.286	----
ZV-5	0.826	48.0	KZV-5	0.016	0.852	57.2
ZV-10	0.926	40.1	KZV-10	0.014	0.910	63.1
ZV-20	1.12	65.6	KZV-20	0.012	0.928	65.6

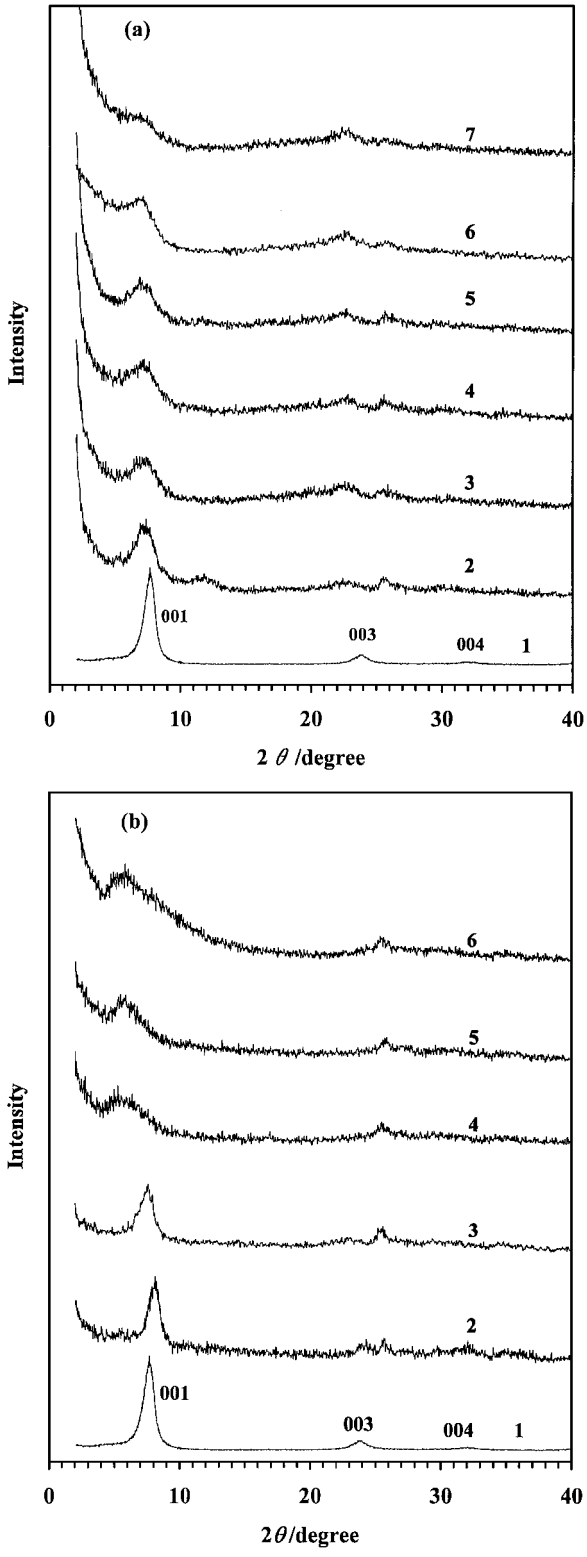

Figure 1 XRD patterns of the layered $V_2O_5{\cdot}nH_2O$ intercalated with ultrafine TiO_2 particles. a: 1, $V_2O_5{\cdot}nH_2O$; 2, TV-0.5; 3, TV-1; 4, TV-2; 5, TV-4; 6, TV-10; 7, TV-20. b: 1, $V_2O_5{\cdot}nH_2O$; 2, K-$V_2O_5{\cdot}nH_2O$; 3, KTV-1; 4, KTV-5; 5, KTV-10; 6, KTV-20.

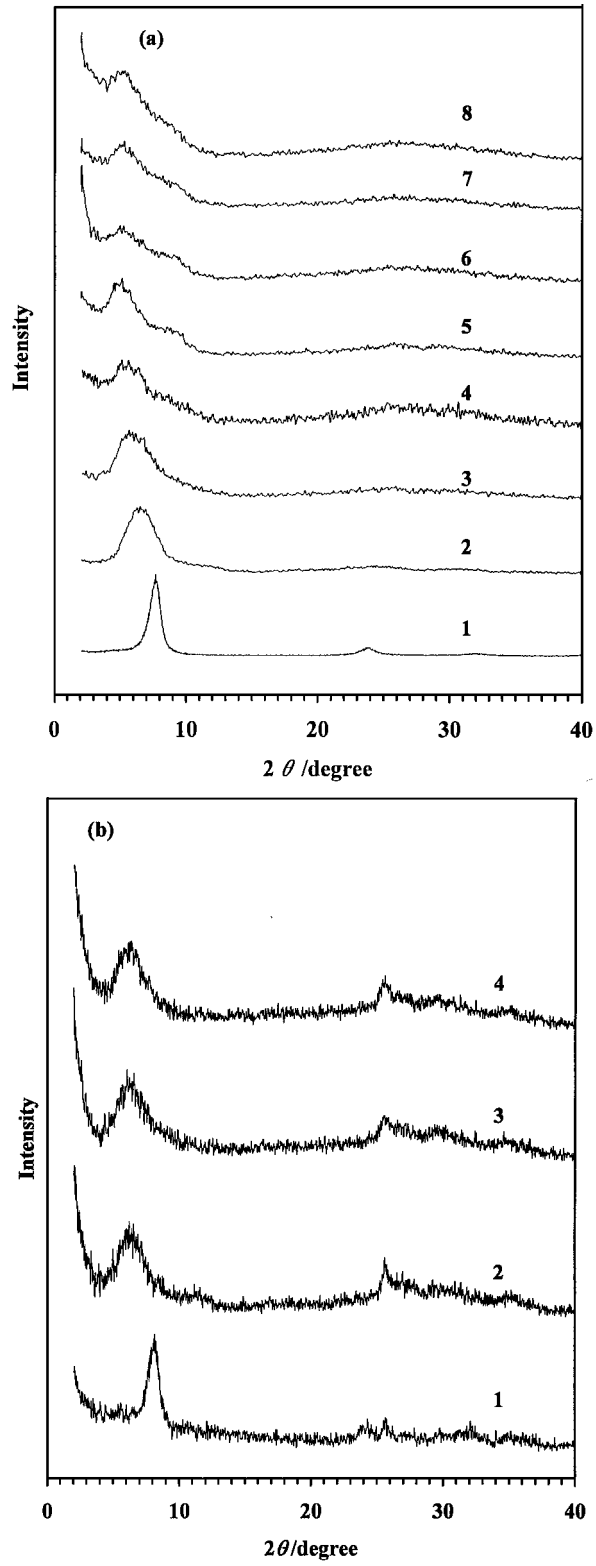

Figure 2 XRD patterns of the layered $V_2O_5{\cdot}nH_2O$ intercalated with ultrafine ZrO_2 particles. a: 1, $V_2O_5{\cdot}nH_2O$; 2, ZV-0.1; 3, ZV-0.3; 4, ZV-0.5; 5, ZV-1; 6, ZV-10; 7, ZV-20. b: 1, $V_2O_5{\cdot}nH_2O$; 2, KZV-5; 3, KZV-10; 4, KZV-20.

samples were apparently exfoliated. It is to be noted from Figs. 2a and b that 002 peak can be slightly seen after 001 peak in both, signifying that the ordering of layer stacking is better than that in the system with TiO_2 particles.

3.2. Texture analysis by N_2 adsorption

The surface and porous properties of the products were studied by N_2 adsorption. Adsorption isotherm for the intrinsic $V_2O_5{\cdot}nH_2O$ is apparently a type II, according to the BDDP definition (Fig. 4a, curve 1) [24], but the *t*-plot suggests a complicated mechanism of the N_2 adsorption. After short linear part, the plot increases gradually and reaches the flat part at a higher *t*-range. The small gradient at the beginning part corresponds to the small surface area of the sample ($7.9\ m^2\ g^{-1}$) and the following increase suggests exfoliation of the layered substance. This is ascribed to the fact that a desorption

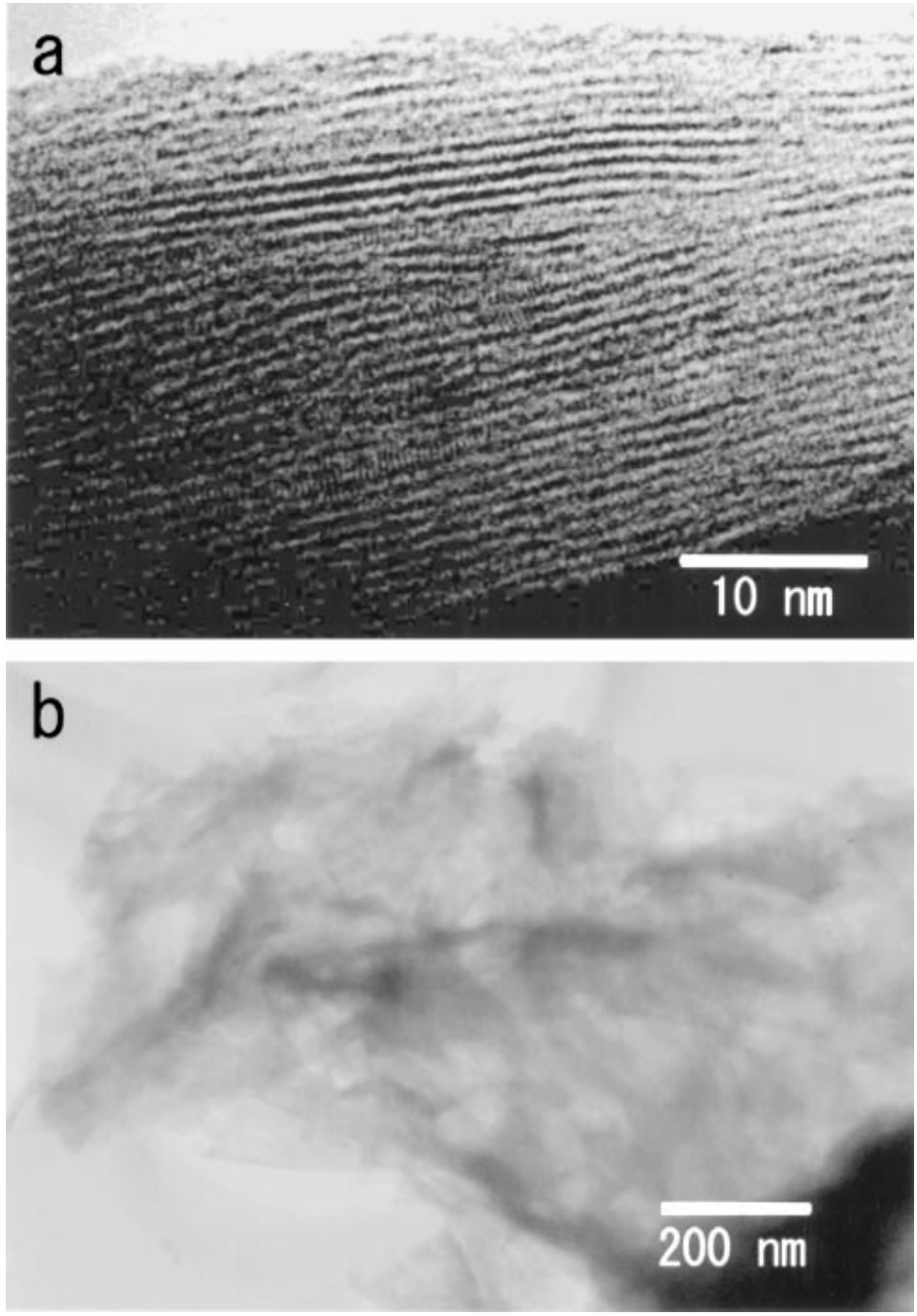

Figure 3 Electron micrographs of the layered $V_2O_5 \cdot nH_2O$ intercalated with ultrafine TiO_2 and ZrO_2 particles. 1, pure $V_2O_5 \cdot nH_2O$; 2, TV-10; 3, KTV-10; 4, ZV-10; 5, KZV-10. (*Continued*).

curve does not run down on the adsorption branch of the isotherm and form a loop. Flattening of the isotherms at higher pressures is due to capillary condensation of N_2.

When a TiO_2 particle is introduced, N_2 adsorption isotherms increase with the TiO_2 ratio and all are type II (Fig. 4a). A *t*-plot analysis of the adsorption isotherms gives almost linear relations for all the TV samples, signifying that there are neither micropores nor mesopores detectable with N_2 (Fig. 4b). Thus, the adsorption of the N_2 gas occurred only on the outer surface of the particle. In other words, the introduction of the fine TiO_2 particles does not form pillars leading to the micropores. The fragmentation of the reaction product, whose layer number is markedly reduced but remains to some extent (Fig. 3a and c), suggests that $V_2O_5 \cdot nH_2O$ sol is still composed of domains with several layer sheets interacting with each other. That is, each domain is separated from others by a positively charged TiO_2 particle surface. As can be seen in Table I, the specific surface area increased by depositing excessively the positively charged TiO_2 particles on the domain surfaces. It is rather curious to find that there could not be seen an indication of interstitials between the layer sheets after exfoliation. This is described later.

In case of the samples KTV, N_2 adsorption is about 2 times larger than in TV and almost unchanged with the mixing ratio of TiO_2 (Table I). It is to be noted that *t*-plot of the adsorption data is slightly convex to the ordinate, indicating that adsorption occurs in the micropores of the products. The K-$V_2O_5 \cdot nH_2O$ is a precipitate formed by coagulating $V_2O_5 \cdot nH_2O$ with K^+ ion

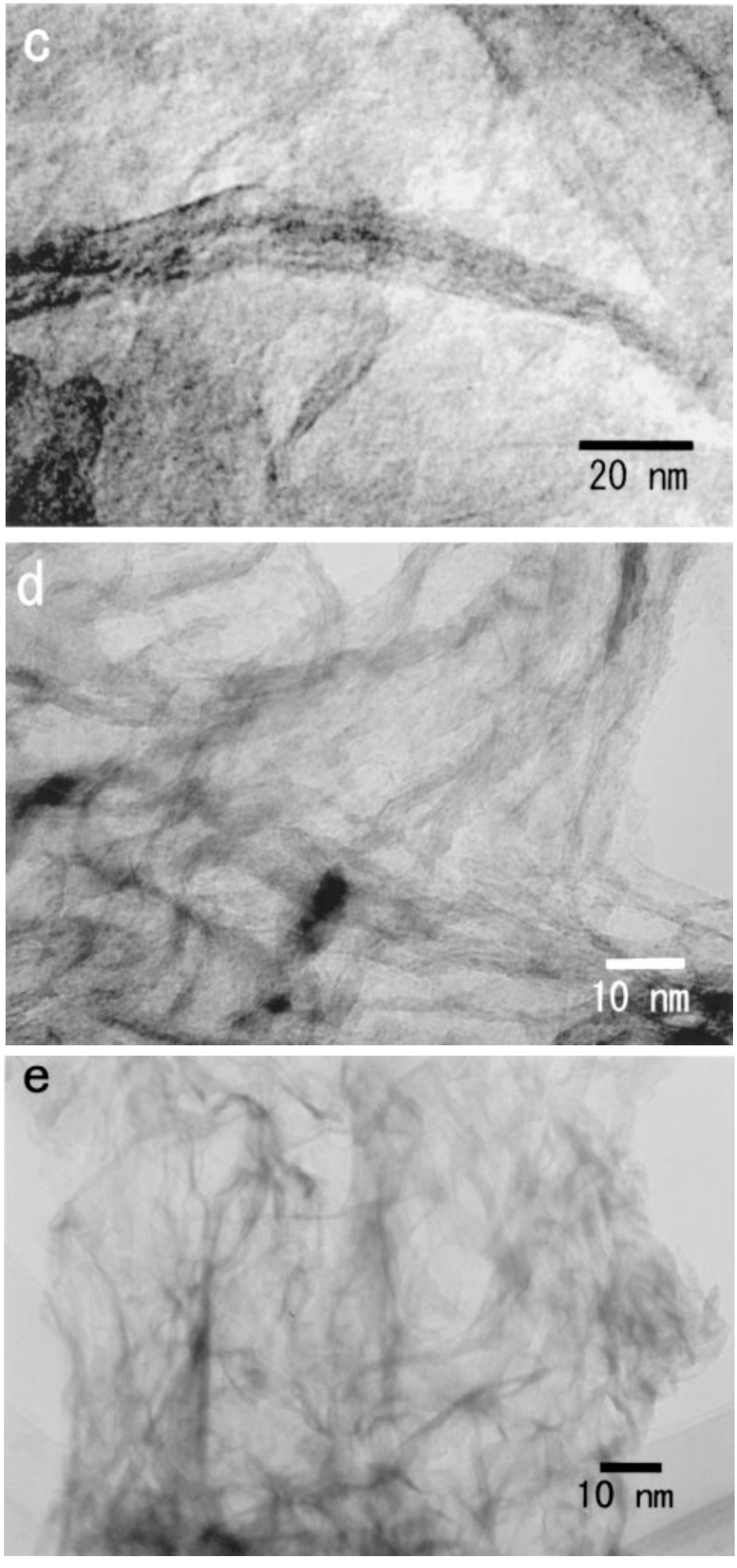

Figure 3 (*Continued*).

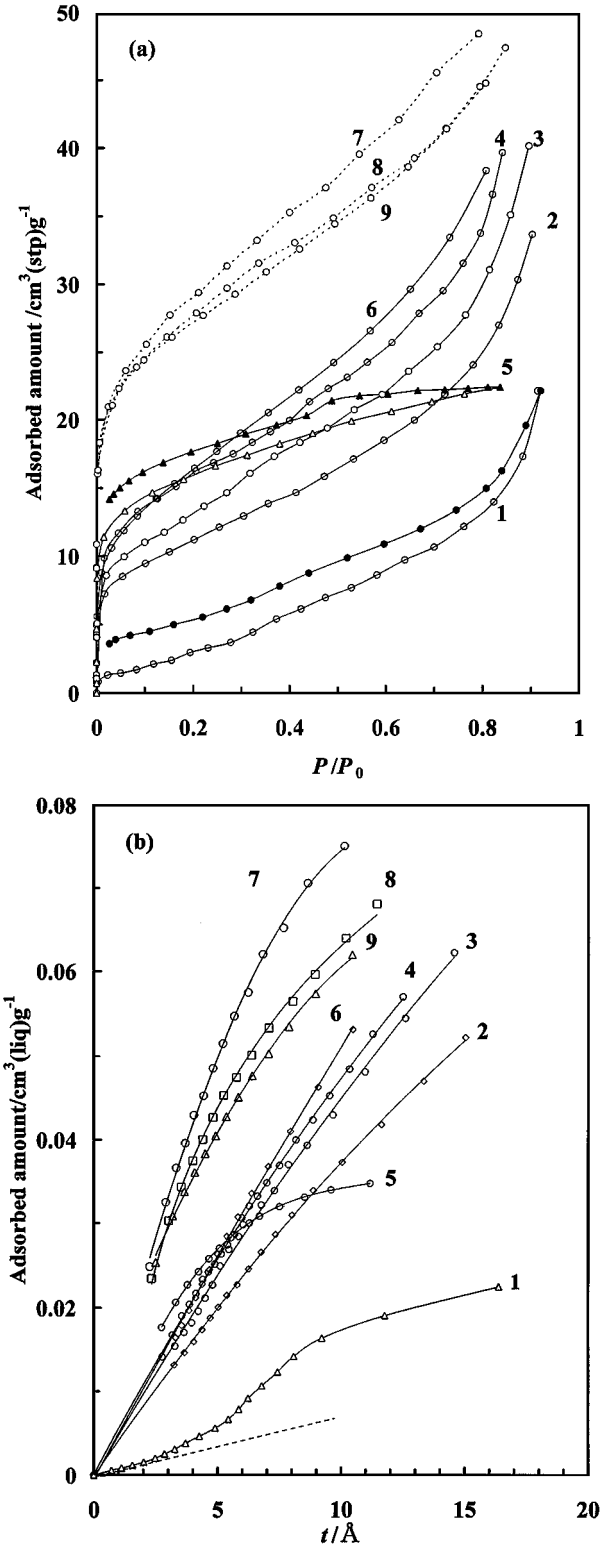

Figure 4 (a) Adsorption isotherms and (b) t-plots of N_2 on the $V_2O_5{\cdot}nH_2O$, TV, and KTV. 1, $V_2O_5{\cdot}nH_2O$; 2, TV-1; 3, TV-4; 4, TV-10; 5, TV-10a; 6, TV-20; 7, KTV-5; 8, KTV-10; 9, KTV-20. Shaded marks show the desorption branch of isotherm.

and thus can be expected to form well-defined stacking [4]. Ion-exchangeably intercalated TiO_2 particles should expand the interlayer distance. According to the XRD pattern of the products in Fig. 1b, indicating the increase of interlayer distance from 11.3 A for intrinsic $V_2O_5{\cdot}nH_2O$ to ~15 Å by intercalation, expanded interlayer distance is too small to accept N_2 molecules in addition to the intercalated TiO_2 particles. In KTV samples, however, the line broadening is significant compared to TV samples, suggesting that pore size is distributed more in the former. Thus, it is reasonable to attribute the micropore formation to the partial expanded parts of layer structures.

The above facts are in contrast to the system composed of clay minerals prepared by Yamanaka *et al.* [7], who did not report the formation of micropores but mesopores by intercalating TiO_2 particles with pores whose size is fairly larger than the expanded layer distances. The absence of the mesopores in the present samples will be ascribed to the difference in the drying processes. In Yamanaka's experiments clays were dried gradually in air, while present samples were all freeze-dried to avoid secondary effects to form interstitial pores by aggregation of the primary particles. A test N_2 adsorption experiment answered to this problem. A TV-10 sample was dried spontaneously from wet sediments in air. The observed adsorption isotherm of this sample was apparently type II but the desorption branch was stepwise as found in the mesoporous system (Fig. 4a, curve 5). In addition, t-plot is convex to the ordinate and suggests that mesopores are not formed (Fig. 4b, curve 5). Furthermore, the desorption run did not come back to the adsorption branch, suggesting separation of layered particles after desorption. Then, it should be understood that spontaneously dried sample is composed of both micropores and mesopores produced as interparticle spaces.

The N_2 adsorption isotherms for the ZV and KZV were similarly type 2 and t-plots for them are all linear, i.e., neither micropores nor mesopores were formed. The surface area of KZV samples is a little bit larger than that of ZV samples. The surface area for each is unvaried when the mixing ratio is changed, which can be directly related to the almost constant stoichiometric amount of ZrO_2 particles between the layers and the idea that layer stacking domains with certain number of layers are present in the $V_2O_5{\cdot}nH_2O$ sol.

3.3. Properties of the layer sheets

Fig. 5 shows the FT-IR spectra for $V_2O_5{\cdot}nH_2O$, TV-5, KTV-5, ZV-5, and KZV-5. It is interesting to find that the spectra for these samples are almost unvaried by intercalation of fine particles from that of pure $V_2O_5{\cdot}nH_2O$ [25]. The V-O stretching vibration along to the b-direction of the layer sheet appearing at 775 cm^{-1} for $V_2O_5{\cdot}nH_2O$ was not affected by intercalation of TiO_2 particles, i.e., in TV-5 and KTV-5. The bands for ZV-5 and KZV-5 gave a slightly higher wave number, 783 cm^{-1}, which suggests that the intimate interactions between layer sheet and ZrO_2 particles are working. On the other hand, V = O stretching vibration along the c-direction at 1014 cm^{-1}, which is normal to the layer sheet is unvaried by interaction with both metal oxide particles.

The chemical bonding state in the layer sheet should reflect the electronic state of them. It is known that intrinsic $V_2O_5{\cdot}nH_2O$ is composed of a small amount of V^{4+} (1-2%) which gives ESR signals of hyperfine 16 peaks by nuclear spins ($I = 7/2$) and anisotropic electric fields, (simulated parameters: $g_{\|} = 1.905$, $A_{\|} = 204.5$, $g_{\perp} = 1.977$, $A_{\perp} = 75.5$) [25]. Fig. 6 shows ESR

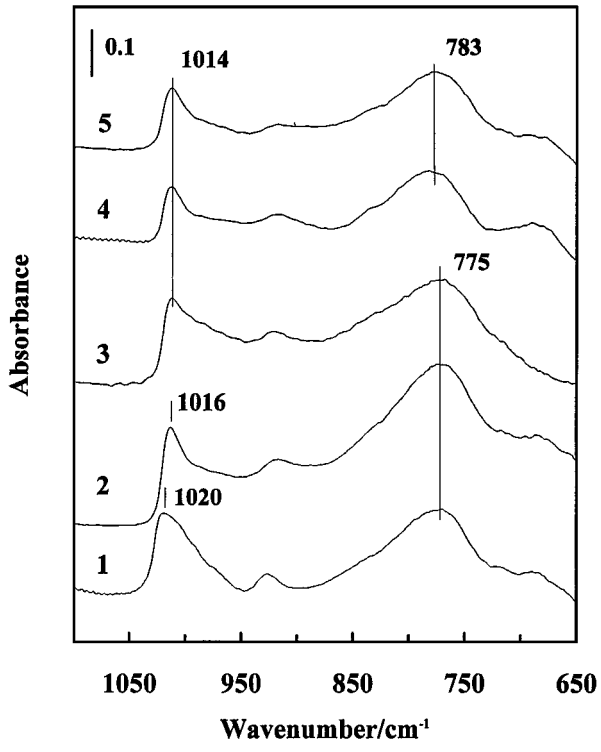

Figure 5 FT-IR spectra of the layered $V_2O_5{\cdot}nH_2O$ intercalated with ultrafine TiO_2 and ZrO_2 particles. Measurements were conducted in a vacuum. 1, pure $V_2O_5{\cdot}nH_2O$; 2, TV-5; 3, KTV-5; 4, ZV-5; 5, KZV-5.

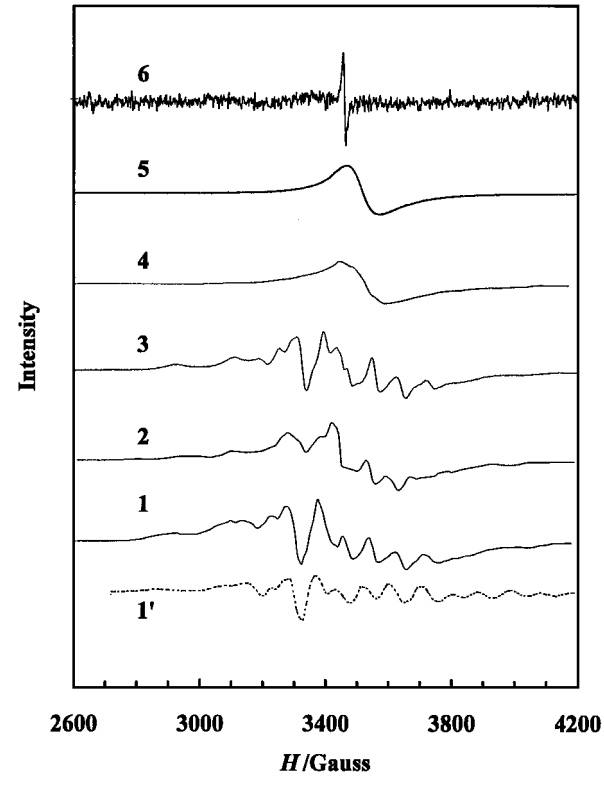

Figure 6 ESR spectra of the layered $V_2O_5{\cdot}nH_2O$ intercalated with ultrafine TiO_2 and ZrO_2 particles. Measurements were conducted in a vacuum. 1, pure $V_2O_5{\cdot}nH_2O$; 1′ simulated for the sample 1; 2, TV-5; 3, KTV-5; 4, ZV-5; 5, KZV-5; ZrO_2.gel.

spectra for the samples TV-5, KTV-5, ZV-5, and KZV-5, together with $V_2O_5{\cdot}nH_2O$ and freeze-dried ZrO_2 gel, all of which have been observed in a vacuum at room temperature. The spectral patterns for TV-5 and KTV-5 are similar to that for intrinsic $V_2O_5{\cdot}nH_2O$, although some differences are seen in the intensity relation. Thus, we can understand that electronic conditions on the V^{4+} in the samples are affected slightly by intercalation of fine TiO_2 particles.

In the cases of ZV and KZV, on the other hand, hyperfine ESR signals characteristic of the V^{4+} in the $V_2O_5{\cdot}nH_2O$ have disappeared and a weak apparently single broad signal appeared instead. A ZrO_2 powder, which was freeze-dried from the sol in the present experiment, gave a small ESR signal due to isolated electrons ($g = 2.0136$). The g value is too high for the electron to be assigned to a bulk Zr^{3+}, $g_{\parallel} = 1.953$ and $g_{\perp} = 1.978$ [26]. Liu *et al.* proposed that this is due to F centers on the surface of fine particles [27]. Although there is no evidence for this, our sample is much smaller particles than theirs and the experimental trend is similar. Allowing for the fact that small clusters have tight contact with the $V_2O_5{\cdot}nH_2O$ layer sheet, it will be reasonable to attribute this line broadening to dipole-dipole interactions between electrons on V^{4+} and the ZrO_2 particle. When remembering back to the sample intercalated with TiO_2, we cannot rule out similar behavior from this sample. However, ESR measurement on the pure TiO_2 gel did not give a spectrum at room temperature but a small one at the temperature of liquid N_2, suggesting the presence of a quite small amount of ESR active electrons in the sample. Thus, above experimental ESR patterns for TV samples are due to electrons in the $V_2O_5{\cdot}nH_2O$ layer sheets.

3.4. Effect of heat treatment

3.4.1. TV and KTV

Thermal properties of the intercalation compounds were studied by DTA-TG measurement, as shown in Fig. 7a. When the TiO_2 particles and ZrO_2 particles are intercalated, DTA curves show a broad change after the initial small part of the endothermic peaks due to the evaporation of weakly adsorbed water. DTA-TG curves for the TV and KTV samples are similar independently of the mixing ratios, so that typical data are shown here. In the case of intrinsic sample (curve 1) both DTA and TG curves are not simple due to the desorption of interlayer water giving different phase with different interlayer distance at each dehydration state [28], i.e., the interlayer property for water molecules is homogeneous. This signifies that the intercalation of fine particles brings in the heterogeneity in the interlayer surface. An exothermic peak appears at around 400°C (curves 3 and 4) after broad endothermic peaks for desorption of H_2O, which is about 50°C higher than 350°C for the intrinsic $V_2O_5{\cdot}nH_2O$ (curve 1). In the case of $V_2O_5{\cdot}nH_2O$, this peak is due to the dehydration accompanied by crystallization to form anhydrous V_2O_5 [19]. Fig. 8a shows the XRD patterns for the samples heated at increasing temperatures. A layered structure is mostly broken or shrunken below 300°C treatment, which is correspondent with a rather clear knee on the DTA result (Fig. 7a curve 3). Above 350°C crystallization of anhydrous V_2O_5 and anatase type TiO_2 have occurred. Electron microscopy visualized rod-like V_2O_5 and fine round anatase particles (not shown). Comparing the thermal properties of the component materials,

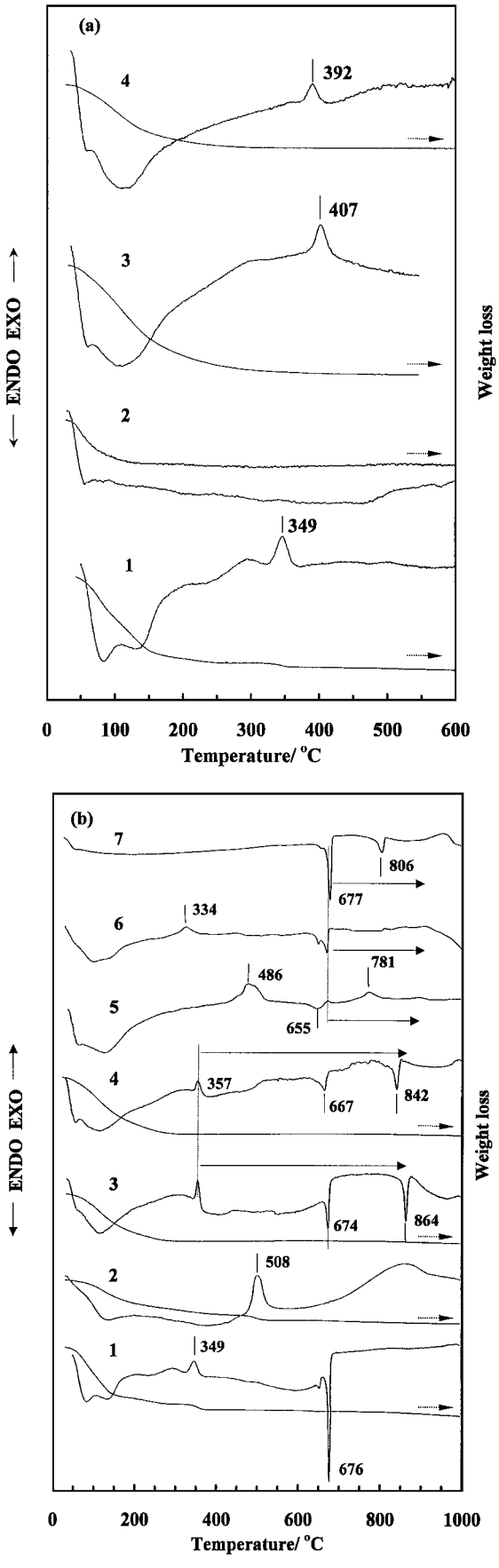

Figure 7 DTA-TG curves of the $V_2O_5 \cdot nH_2O$ intercalated with ultrafine TiO_2 and ZrO_2. (a) 1, pure $V_2O_5 \cdot nH_2O$; 2. TiO_2 gel; 3, TV-5; 4, KTV-5. (b) 1, pure $V_2O_5 \cdot nH_2O$; 2. ZrO_2 gel; 3, ZV-5; 4, KZV-5; 5, mixture of ZrO_2 gel and anhydrous V_2O_5; 6, mixture of anhydrous ZrO_2 and V_2O_5 gel; 7, mixture of anhydrous ZrO_2 and V_2O_5. The ranges illustrated by "→" indicated the temperature range at which ZrV_2O_7 are formed. Weight changes (directed by broken arrows) are illustrated by arbitrary unit to show just dehydration processes.

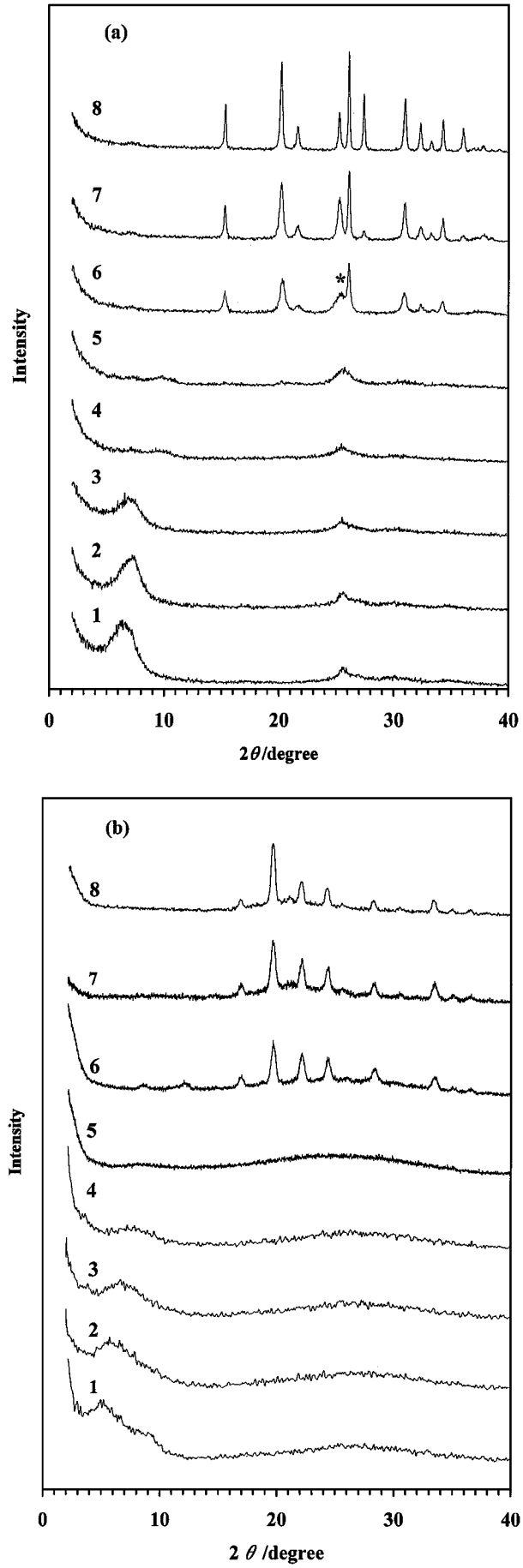

Figure 8 Effect of heating on the XRD patterns of (a) TV-5 and (b) ZV-5. Heating temperatures (°C) a: 1, room temperature; 2, 100; 3, 200; 4, 300; 5, 350; 6, 400; 7, 500; 8, 600. b: 1, room temperature; 2, 50; 3, 100; 4, 200; 5, 300; 6, 350; 7, 500; 8, 600. *shows the 101 diffraction peak for the anatase.

i.e., an exothermic peak at 350°C for $V_2O_5 \cdot nH_2O$ (curve 1) and an absence of detectable signal for TiO_2 (curve 2) in the temperature range around here, the exothermic peak at 400°C can be easily ascribed to dehydration and crystallization of $V_2O_5 \cdot nH_2O$ into anhydrous V_2O_5. That is, the crystallization process was inhibited by the presence of fine TiO_2 particles. This is rather general trend with $V_2O_5 \cdot nH_2O$ when cationic species are ion-exchangeably introduced [28]. The reason is that the crystallization of V_2O_5 is preceded by the dehydration of the starting material consuming structural OHs. When protons of OHs are lost by an ion-exchange reaction, crystallization should be led from the dehydrated structure that is carried about by diffusion of component atoms of V and O. This idea is supported by the TG-DTA analyses in Fig. 7a and b. Allowing for the melting point of at 676°C, it is reasonable to anticipate the increase in crystallization temperature. These results agree with the fact that a homogeneous solid solution or compound is not formed between V_2O_5 and TiO_2 in the ambient conditions up to higher temperature.

The N_2 adsorption behavior on the TV samples upon heat treatment was for the nonporous samples. The specific surface area change is shown as a function of temperature for the typical examples TV-10 (Fig. 9). The surface area decreased almost linearly with temperature. In contrast, the larger surface area for KTV-10 has decreased slowly to around 300°C, above which it dropped, although the appearance of the N_2 adsorption isotherms are all type II (Fig. 10a), *t*-plots give convex curves to the ordinate up to 300°C and a linear relation is followed (Fig. 10b). This behavior is reflected by the surface area change with temperature. Thus, high surface area is due to the additional adsorption in the micropores.

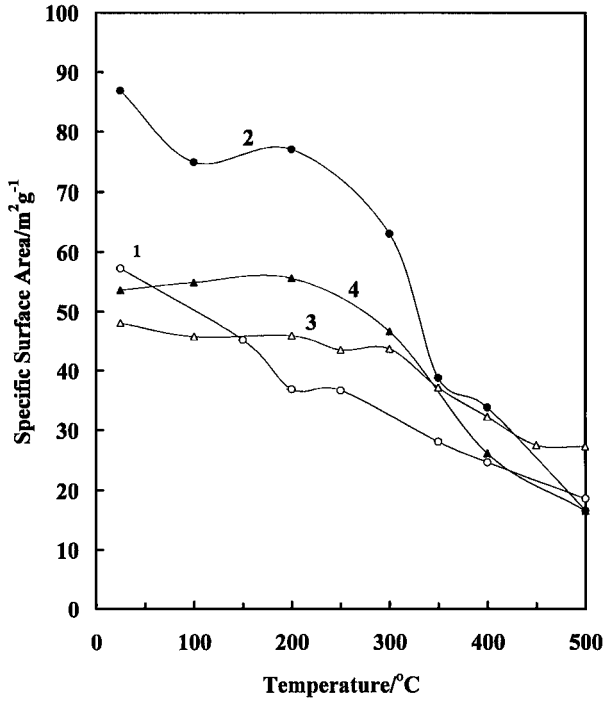

Figure 9 Effect of heating on the surface areas of the $V_2O_5 \cdot nH_2O$ intercalated with ultrafine TiO_2 and ZrO_2. 1, TV-10; 2, KTV-10; 3, ZV-5; 4, KZV-5.

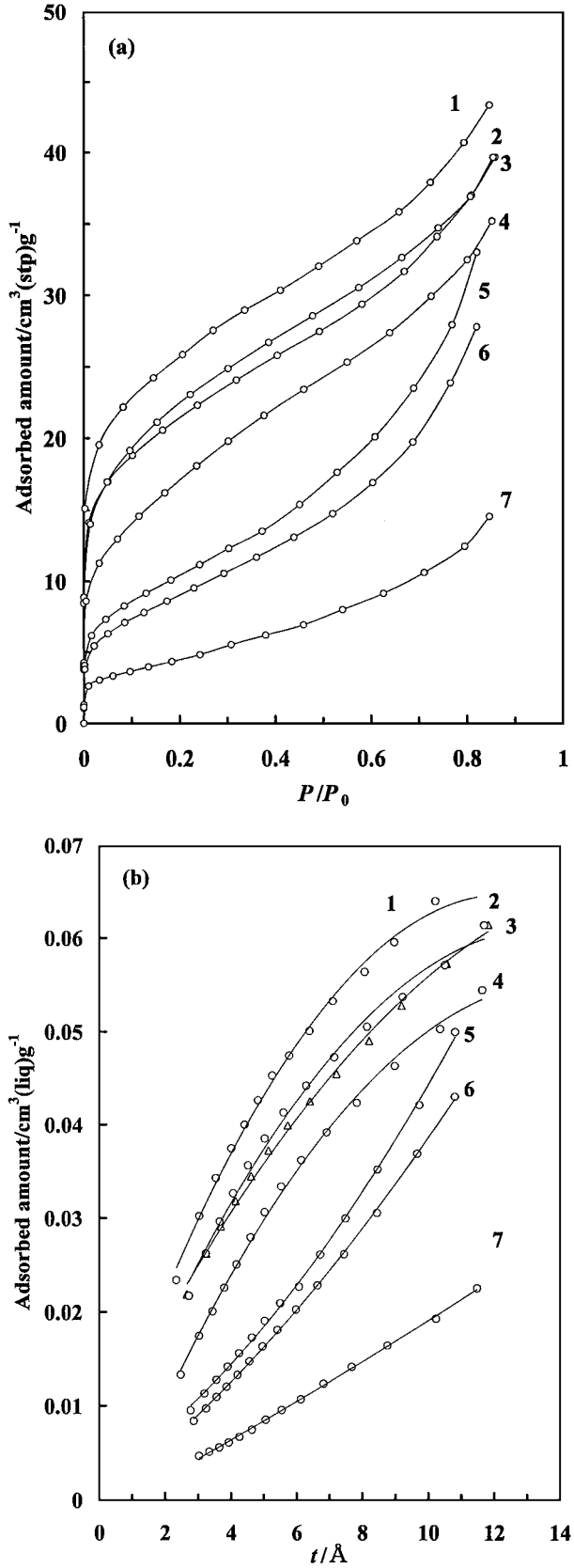

Figure 10 Effect of heating on the (a) adsorption isotherms and (b) *t*-plots of N_2 for KTV-10. Heating temperatures (°C): 1, room temperature; 2, 100; 3, 200; 3, 300; 4, 350; 5, 400; 6, 500.

3.4.2. ZV and KZV

DTA-TG curves for ZV and KZV are unvaried independently of the mixing ratios of the sols, $ZrO_2/V_2O_5 > 5$ (Fig. 7b). The DTA curve for ZV-5 (curve 3) show a clear exothermic peak at 357°C and two sharp endothermic peaks at 674°C and 864°C; the KZV-5 displaces

the last peak a little to lower temperature (curve 4). XRD patterns of the heated ZV show clearly the formation of cubic ZrV_2O_7 after 350°C (Fig. 8b) which is slightly lower than the temperature determined by DTA measurements, probably because the latter is dynamically determined. The atomic ratio of 1 : 2 for Zr : V in the Table II can be directly related to the heated material ZrV_2O_7. Furthermore, allowing for the fact that $V_2O_5{\cdot}nH_2O$ is dehydrated at 349°C, it is reasonable to conclude that the formation of ZrV_2O_7 is invoked by the dehydration of $V_2O_5{\cdot}nH_2O$ (curve 1) and that dehydration of ZrO_2 xerogel is not a starter for this reaction (curve 2).

ZrV_2O_7 is a typical sample that expresses the thermal expansion change from positive to negative, which is accompanied by the cubic-cubic phase change [29]. Thus, this material is of special interest for solid state chemistry. The conventional method to prepare ZrV_2O_7 was compared with the present case. Anhydrous V_2O_5 and ZrO_2, $V_2O_5{\cdot}nH_2O$ and ZrO_2 gel were mixed interchangeably (curves 5–7). A temperature to lead a common chemical process is around 650–680°C above which ZrV_2O_7 phase can be observed. Appearance of complicated peaks above this temperature is due to the appearance of the multiphases including a liquid solution [30]. This is out of scope in the present work. Anyhow, the solid-state reaction started with the melting of V_2O_5 as can be anticipated by the endothermic peak for melting at 676°C (curve 1). Thus, the formation of at 357°C is extremely lower than that by the solid-state reaction.

These facts signify that ZrO_2 particles are distributed homogeneously between the $V_2O_5{\cdot}nH_2O$ sheets and the reactivity of vanadium ions produced by dehydration at 350°C gives a low reaction temperature.

As seen in Fig. 9, the surface areas of the ZV and KZV samples are not so much different from each other and change with heating temperature is parallel. The surface area is maintained constant up to 300°C. Above 300°C it decreases gradually with temperature although the crystal structure changes markedly. This signifies that the discreteness of the exfoliated particles is slowly lost with temperature. These changes are rather parallel with the structural change upon heating. Allowing for the weight losses at rather low temperatures of all the samples, it is also concluded that a flat dry surface can be obtained around at 300°C. The surface properties of these samples are not clarified but are to be studied for the possibility as oxidation catalyst.

3.5. Intercalation mechanism of fine metal oxide particles in the $V_2O_5{\cdot}nH_2O$

Lastly, intercalation mechanism is discussed shortly. In the present systems, all the reactions were conducted at high proton concentrations, which is adjusted to disperse well defined fine particles of TiO_2, and ZrO_2. PZC values for V_2O_5, TiO_2, and ZrO_2 are higher than pH values of the reaction system (>0) and thus surface charges of all the substances are positive. Accordingly, a simple ion-exchange model cannot be applied in the present case. It will be possible to consider that metal oxide particles are sandwiched simply by van der Waals force with $V_2O_5{\cdot}nH_2O$ under high ionic strength. This situation is similar to the system with clay minerals [7]. Detailed analysis of this mechanism awaits further study.

4. Conclusions

1. TiO_2 particles are intercalated in the $V_2O_5{\cdot}nH_2O$ to expand interlayer distances, by which the surface area is increased about 8 times larger than that of $V_2O_5{\cdot}nH_2O$. K-type $V_2O_5{\cdot}nH_2O$ is acceptable for TiO_2 particles, by which micropores are formed and surface areas are increased by about 2 times from that in the former. ZrO_2 particles are intercalated between the layers of $V_2O_5{\cdot}nH_2O$ and K-type $V_2O_5{\cdot}nH_2O$ as well as TiO_2 particles. The intercalation compounds formed have an almost constant ratio, $ZrO_2/V_2O_5 = 1$ independent of the mixing ratios, suggesting that some stoichiometric reaction has been working between reactants rather than simple ion-exchange reaction.

2. Thermal property changes of the $V_2O_5{\cdot}nH_2O$-TiO_2 system are decided by the solid properties of the component oxides. When the layered structure is broken at the temperature at which anhydrous V_2O_5 and anatase are grown, the surface area has decreased markedly. Similar change occurs in the $V_2O_5{\cdot}nH_2O$-ZrO_2 system at the temperature at which $V_2O_5{\cdot}nH_2O$ is decomposed to form Zr V_2O_7. This temperature is much lower than that by the conventional method of mixing and heating component oxide powders, due to the fact that the mixing process is saved much at low temperatures.

Acknowledgements

Financial support has promoted the present research significantly: a Special Grant for Cooperative Research Administered by the Japanese Private School Promotion Foundation and a Grand in Aid for Scientific Research, No. 09874148 are heartily appreciated.

References

1. N. BAFFIER, P. ALDEBERT, J. LIVAGE and H. W. HAESSLIN, *J. Colloid Interface Sci.* **141** (1991) 467.
2. T. KAMIYAMA, T. ITOH and K. SUZUKI, *J. Non-Crys. Solids* **100** (1988) 466.
3. T. TACHI, A. KATO, H. YAMASHITA and S. MATSUDA, *Nippon Kagaku Kaishi* (1992) 689.
4. S. KITTAKA, N. UCHIDA, M. KATAYAMA, A. DOI and M. FUKUHARA, *Colloid Polym. Sci.* **269** (1991) 835.
5. S. KITTAKA, N. FUKUHARA and H. SUMIDA, *J. Chem. Soc. Faraday Trans.* **89** (1993) 3827.
6. J. STERLE, *Clays Clay Miner.* **34** (1986) 658.
7. S. YAMANAKA, T. NISHIHARA and M. HATTORI, *Mat. Chem. Phys.* **17** (1987) 87.
8. Y. KITAYAMA, T. KODAMA, M. ABE and H. SHIMOTSUMA and Y. MATSUDA, *J. Porous Matr.* **5** (1998) 121.
9. M. L. OCCELLI and R. M. TIUDWA, *Clays Clay Miner.* **31** (1983) 22.
10. E. KIKUCHI, T. MATSUDA, H. FUJIKI and T. MORITA, *Appl. Catal.* **11** (1984) 331.
11. G. BUSCA, G. CENTI, L. MARCHETTI and F. TRIFIRO, *Langmuir* **2** (1986) 568.
12. B. L. DUFFY, H. E. CURRY-HYDE, N. W. CANT and P. F. NELSON, *J. Phys. Chem.* **98** (1994) 7153.
13. H. MIYATA, M. KOHNO, T. ONO, T. OHNO and F. HATAYAMA, *J. Chem. Soc. Faraday Trans. I* **85** (1989) 3663.

14. J. M. JEHNG, *J. Phys. Chem. B* **102** (1998) 5816.
15. M. GALÁN-FERERES, R. MARISCAL, L. J. ALEMANY, J. L. G. FIERRO and J. A. ANDERSON, *J. Chem. Soc. Faraday Trans.* **90** (1994) 3711.
16. Y. OKA, N. YAMAMOTO and T. YAO, *Solid State Ionics* **57** (1992) 103.
17. S. KITTAKA, K. MATSUNO and H. AKASHI, *J. Solid State Chem.* **142** (1991) 835.
18. S. KITTAKA, Y. YATA, K. MATSUNO and H. NISHIDO, *J. Mater. Sci.* **35** (2000) 1.
19. S. KITTAKA, Y. AYATSUKA, K. OHTANI and N. UCHIDA, *J. Chem. Soc. Faraday Trans. I.* **85** (1989) 3825.
20. F. A. COTTON and G. WILKINSON, "Advanced Inorganic Chemistry," 3rd ed. (John Wiley and Sons, N. Y., 1972) p. 931.
21. G. A. PARKS, *Chem. Rev.* **65** (1965) 177.
22. R. KONDO and M. DAIMON, *Hyomen* **12** (1974) 377.
23. N. GHARBI, C. SANCHEZ, J. LIVAGE, J. LEMERLE, L. NÉJEM and J. LEFEBVRE, *Inorg. Chem.* **21** (1982) 2758.
24. S. BRUNAUER, L. S. DEMMING, W. E. DEMMING and E. TELLER, *J. Amer. Chem. Soc.* **62** (1940) 1723.
25. S. KITTAKA, H. HAMAGUCHI, T. UMEZU, T. ENDOH and T. TAKENAKA, *Langmuir* **13** (1997) 1352.
26. C. MORTERRA, E. GIAMELLO, L. ORIO and M. VOLANTE, *J. Phys. Chem.* **94** (1990) 3111.
27. H. LIU, L. FENG, X. ZHANG and Q. XUE, *ibid.* **99** (1995) 332.
28. S. KITTAKA, N. UCHIDA, T. KIHARA, T. SUETSUGI and T. SASAKI, *Langmuir* **8** (1992) 245.
29. V. KORTHUIS, N. KHOSROVANI, A. W. SLEIGHT, N. ROBERTS, R. DUPREE and W. W. WARREN, JR., *Chem. Mater.* **7** (1995) 412.
30. V. CIRILLI, A. BURDESE and C. BRISI, *Atti Accad. Sci. Torino* **95** (1961) 14.

Received 11 April
and accepted 13 November 2000